A Variational Study on BRDF Reconstruction in a Structured Light Scanner

Jannik Boll Nielsen, Jonathan Dyssel Stets, Rasmus Ahrenkiel Lyngby,
Henrik Aanæs, Anders Bjorholm Dahl, Jeppe Revall Frisvad
Technical University of Denmark
http://eco3d.compute.dtu.dk/

Abstract

Time-efficient acquisition of reflectance behavior together with surface geometry is a challenging problem. In this study, we investigate the impact of system parameter uncertainties when incorporating a data-driven BRDF reconstruction approach into the standard pipeline of a structured light scanning system. The parameters investigated include geometric detail of scanned objects; vertex positions and normals; and position and intensity of light sources. To have full control of uncertainties, experiments are carried out in a simulated environment, mimicking an actual structured light scanning setup. Results show that while uncertainties in vertex positions and normals have a high impact on the quality of reconstructed BRDFs, object geometry and light source properties have very little influence on the reconstructed BRDFs. With this analysis, practitioners now have insight in the tolerances required for accurate BRDF acquisition to work.

1. Introduction

The topic of accurate appearance capture and digitization is gaining attention in areas like the movie and gaming industries [9], preservation of cultural heritage [6], and quality assurance in production [18]. These applications demand automatic and fast systems that can acquire full and accurate appearance, including both radiometry and geometry. In combination, these two components define appearance, and numerous methods have been proposed for their acquisition. Capturing high quality geometric models of real world objects is today a well-addressed problem with many good solutions. Different technologies exist such as structured light (SL) scanners, multi-view stereo, or time-of-flight, each having their own advantages and disadvantages. With respect to radiometric properties, techniques such as goniometric setups, curved mirror configurations, and light domes can be used for accurately estimating bidirectional reflectance distribution functions (BRDFs) of simple, often flat, geometries. However, robust approaches for jointly estimating radiometry and geometry are few and often require advanced and expensive setups or produce low quality results.

In this paper we investigate how a SL scanner, designed for high quality geometry acquisition, can be modified with few adjustments to also capture reflectance samples. Thus, the scanner can also sample the BRDF of a scanned object and reconstruct it using state of the art BRDF reconstruction methods. Using this system as an offset, we investigate the influence on BRDF estimation caused by various system uncertainties. The uncertainties investigated include: geometric complexity of the scanned object, vertex position and normal, and light source position and intensity. Our aim is to gain insight into how BRDF reconstruction is affected by various error sources and uncertainties. As a main result, we provide a lookup table for system designers, telling them the system specifications required for correctly estimating BRDFs in a given material/geometry configuration. In order to ensure full control of all uncertainties, the experiment is designed as a simulation of an SL scanner system. The simulation is based on real world parameters from an actual SL scanning system, as well as real measured BRDFs from the MERL database [17].

Although this study focuses on an SL scanning system, we believe that the proposed modification, as well as the insights into the influence of error sources, applies to most 3D scanning systems where an image-forming sensor and a light source is present. Likewise, while we apply the BRDF reconstruction framework of Nielsen et al. [20], we expect other BRDF modeling frameworks with strong priors to be applicable as well.

2. Related Work

A multitude of techniques exist for acquiring shape and appearance [30]. Most techniques are time consuming or require highly specialized equipment. In the following, we relate our work to instrumental setups that are similar to the one we propose. Our setup is a structured light 3D scanner setup with two cameras, a projector light source, and a turntable. An additional LED source is added to our setup.

Nielsen, J. B., Stets, J. D., Lyngby, R. A., Aanæs, H., Dahl, A. B., and Frisvad, J. R. A variational study on BRDF reconstruction in a structured light scanner. In *Proceedings of IEEE International Conference on Computer Vision Workshop (ICCVW 2017)*, pp. 143-152. October 2017.
https://doi.org/10.1109/ICCVW.2017.25

An example of early work investigating the acquisition of shape and reflectance properties using images is that of Ikeuchi and Sato [11]. They fit the Torrance-Sparrow BRDF model [28] to samples obtained from a range image and a brightness image. To investigate the convergence of their method to true values (robustness), they do a simulation study based on rendered images with different noise levels applied. This enables them to draw important conclusions with respect to the sensitivity and range of applicability of their method. Unfortunately, it seems that such simulation studies are very uncommon in subsequent work in this area. To fill this gap, we present a simulation study of this kind for our more contemporary acquisition technique.

The idea of a camera, a light source, and a turntable for joint acquisition of shape and appearance (surface geometry and BRDF) was pioneered by Lu and Little [15]. They use a collimated source and estimate the BRDF for (near) zero half-angle by finding the points of maximum intensity and tracking them as the object turns around its axis. After this, they acquire the surface geometry using a shape from shading approach. Their approach requires assumption of a smooth object and a uniform BRDF across the object surface. The instrument we consider is similar in complexity, but based on a structured light setup with a projector light source and two cameras (stereo). We also flip the procedure and acquire shape using structured light, and then we estimate a full isotropic BRDF.

It is interesting to note that Lu and Little [15] try perturbations of depth and rotation axis to investigate robustness of their technique. In addition, they indicate that experiments on synthetic images to perform a more in-depth investigation would be appropriate. Nevertheless, we are unable to find such an investigation in the work following that of Lu and Little. Our goal is thus to provide one.

Based on robot arm sample rotation and a structured light range scanner, Sato and Ikeuchi [24] extend their earlier (range and brightness image) technique to include scan of the full geometry of an object and estimation of its spatially varying reflectance properties. The reflectance properties are, however, parameters in an analytic BRDF model and no BRDF ground truth is available for validation. Marschner et al. [16] propose a similar technique, but based on a handheld camera and the Lafortune BRDF model [13]. Employing a more conventional structured light 3D scanner (or a computed tomography scanner) to obtain surface geometry, Lensch et al. [14] extend the technique to acquire Lafortune model parameters for spatially varying BRDFs.

Krzesłowski et al. [12] present a structured light scanner with added LED sources for integrated acquisition of BRDF and surface geometry. However, they fit their sampled BRDF data to the Blinn-Phong model [2, 22], which only provides a good BRDF fit for a limited range of materials [19]. The structured light scan provides a sparse sampling of the BRDF per sample point in the scanned surface geometry. The Blinn-Phong model is fitted to this sparse set of BRDF samples. The acquisition approach we investigate is similar, but we do a simulation study to identify the impact of different potential error sources. We limit our study to an object with just one BRDF across the object surface, and we use the BRDF model of Nielsen et al. [20].

Using a beam splitter to have coaxial camera and projector light source, Holroyd et al. [10] develop a gonioreflectometer which can also acquire the surface geometry using structured light. While this technique delivers high quality acquisitions, it is not a time-efficient approach like a structured light setup. Sitnik et al. [27] propose a faster integrated measurement system with a single image sensor. Here, a multi-spectral camera is combined with a projector and a grid of 16 broadband light sources to capture both the 3D geometry and multi-spectral light intensity information. In another complex setup, Tunwattanapong et al. [29] propose a rotating light arc providing spherical harmonic illumination used together with five cameras to reconstruct reflectance maps. The geometry is then reconstructed using multi-view stereo based on the diffuse and specular reflectance maps. Finally, Schwartz et al. [25] propose a system, based on SL and HDR imaging, for measuring bidirectional texure functions (BTFs) using a light dome composed of 188 LEDs, four projectors, eleven cameras and a rotation stage. The complexity of these instrumental setups is significantly higher than the SL setup that we propose.

3. Implementation

In this study, the BRDF estimation process revolves around a structured light scanning system like the one illustrated in figure 1. The system is composed of two cameras used for triangulation, a projector for projecting an encoding pattern, a rotation stage for rotating a sample, and a scene light. The principles behind the approach should be applicable to any 3D scanning system comprised of components including an image-forming sensor and a light source. In the following subsections, the modified SL capturing pipeline is outlined along with the reconstruction method. The implementation of the modifications required for a structured light scanning system to estimate BRDFs is fairly straightforward in practice, however, to ensure full control of all variables in the study, as well as avoiding unforeseen noise sources, the reflectance acquisition part of the pipeline is here simulated. Below, the details of this simulation process will also be covered.

3.1. Capture Pipeline

The principles behind estimating a BRDF in the SL pipeline are based on the assumption that the BRDF can be observed under a sufficient number of view/light configurations. We need enough to confidently fit a model to the ob-

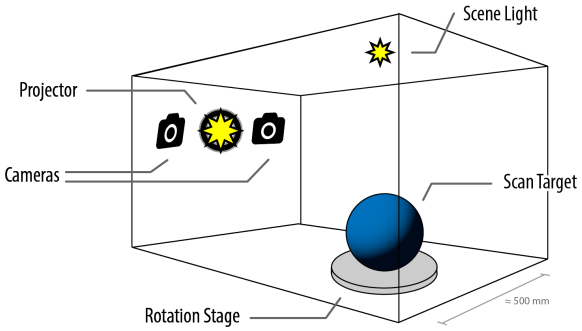

Figure 1: Structured light scanning system consisting of two cameras used for triangulation, a projector for projecting an encoded pattern, a rotation stage for rotating the sample, and a scene light.

servations. Enough configurations are obtained in scenarios where a scanned object, with a sufficiently varying surface geometry, consists of a homogeneous material and is rotated during the capturing process. Any point on the surface will thus be observed under different view/light configurations, and with a sufficiently large number of points with unique surface normals, a sufficiently large number of BRDF samples can be acquired for reconstruction.

Clearly, the full four-dimensional space spanned by the BRDF will not be covered by these observations, let alone due to the fixed baseline between light source (projector) and observer (cameras), which corresponds to a fixed difference angle (θ_d) in the Rusinkiewicz parametrization [23]. Even in a better posed scenario as figure 1, where an additional scene light is present, the BRDF space is still very sparsely sampled. Nonetheless, a sufficient number of observations can in fact be acquired through this process if we use a strong prior when fitting a BRDF model.

The SL scanning pipeline involves projecting an encoding pattern onto the target object and triangulating the encoded pixels seen by the camera(s). This is sometimes followed by a rotation of the sample, after which the scanning is repeated. The modification to the standard SL scanning pipeline is simple and consists only in capturing a high dynamic range (HDR) image of the sample. This is done before the sample is rotated (or removed) using the triangulation camera(s) and a fully lit projector. If a scene light is present, as it is here, an additional HDR image is captured under its illumination. With the captured HDR images, it is possible in post-processing to reproject the captured vertices onto these and acquire a radiance value. With knowledge of vertex normal, camera position, light source position, and light source intensity, this radiance value may be converted into a BRDF sample, defined by

$$f_r\left(\boldsymbol{\omega}_i, \boldsymbol{\omega}_r\right) = \frac{dL_r\left(\boldsymbol{\omega}_r\right)}{dE_i\left(\boldsymbol{\omega}_i\right)}, \tag{1}$$

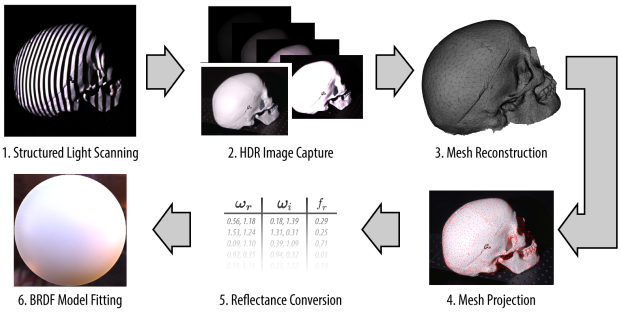

Figure 2: Geometry and BRDF capture pipeline in a structured light scanning system.

which is the ratio between the radiance reflected off a surface in a specific direction and the irradiance hitting a surface from another specific direction.

The overall capturing pipeline is depicted in figure 2. The pipeline consists of:

1. Structured light scanning
2. HDR image capture
3. Mesh reconstruction
4. Mesh projection onto HDR images
5. Per vertex HDR intensity to reflectance conversion
6. BRDF model fitting

In step 1, a traditional 3D scanning is carried out, in this case using structured light. Before altering anything in the scene in any way, e.g. by rotating or removing the sample, an HDR image is captured in step 2 using the multiple exposure approach of Debevec et al. [3]. This ensures a floating point precision image conforming with the scanned geometry and camera calibration of the SL scanner. The acquisition part is followed by post processing, initialized with a meshing in step 3 of the acquired point cloud. As will later become apparent, a mesh is required for filtering purposes. In step 4, the mesh is projected onto the HDR images, assigning every vertex with an HDR intensity. All vertex intensities are in step 5 converted to reflectance values based on scene geometry, and finally in step 6 a BRDF model is fitted to the observed BRDF samples.

3.1.1 Structured Light Scanner

In order to provide a thorough description of our method, we briefly outline our SL scanning strategy. Please note that this is by no means a complete description. For specific details, we refer to the work of others [8, 33, 4].

SL scanning is a form of stereo vision. Essentially, stereo vision is the process of reconstructing the 3D shape of an object by using a set of cameras as protractors. The pixel positions, and thereby the incident angles, of a given 3D

point are found in the camera images. From knowing the mutual transformations between the cameras, the 3D position of the point can be computed based on trigonometry. The key difficulty is finding corresponding points in the images. SL based techniques seek to lower the complexity of this correspondence problem by projecting a known pattern onto the reconstruction object. There are a plethora of encoding strategies available [5], but they all seek to assign unique ID numbers to pixels based on their distance from the projector. These ID numbers are then used to determine pixel correspondences, and from that compute the depth of the surface under the pixels.

Based on the conclusions made by Eiríksson et al. [4], we have selected a scanner system composed of two cameras and one projector which uses the phase shifting (PS) encoding strategy [7]. In short, the projector projects a series of spatially distributed gray-scale sinusoidal patterns onto the target surface. Each pattern has a given frequency and phase shift. We use three frequencies with up to 32 phase shifts per frequency for a total of 64 patterns.

3.1.2 Vertex Reflectance Assignment

From the calibration of the SL scanning system, the intrinsics and extrinsics have been determined. Commonly these are described by a pinhole camera model with a projection matrix $\boldsymbol{P}$ given as:

$$\boldsymbol{P} = \boldsymbol{K}\left[\boldsymbol{R}\,\boldsymbol{t}\right], \tag{2}$$

with $\boldsymbol{R}$ and $\boldsymbol{t}$ being the rotation and translation of the camera respectively, and $\boldsymbol{K}$ being the intrinsic parameters of the camera [34]. With this, any 3D point in homogeneous coordinates, $\boldsymbol{q}$, may be projected onto the cameras 2D image plane by:

$$\hat{\boldsymbol{q}} = \boldsymbol{P}\boldsymbol{q}. \tag{3}$$

Thus, any vertex from a scanned object may be reprojected onto its corresponding HDR image and have a specific radiance RGB value assigned to it. By calibration with e.g. Spectralon, the light intensity at the sample can be predetermined, and often this intensity can be assumed constant over the physical span of the sample. With this prior knowledge, and correcting with the cosine between light and vertex normal, the vertex radiance value may be converted into a BRDF value:

$$f_r = \frac{\texttt{HDR}(\boldsymbol{P}\boldsymbol{v}_{\texttt{position}})}{(\boldsymbol{\omega}_i \cdot \boldsymbol{v}_{\texttt{normal}})\, I}, \tag{4}$$

where $\texttt{HDR}(\hat{\boldsymbol{q}})$ is the HDR radiance value at position $\hat{\boldsymbol{q}}$, $\boldsymbol{v}$ is the vertex, $\boldsymbol{\omega}_i$ is the normalized light direction, and I is the predetermined light intensity at the position of the scanned sample.

Note that some vertices may be projected into shadow regions in the HDR image. In order to avoid this, two tests are employed. First, all vertices with a normal facing away from the camera or light are removed, this is the case when $\boldsymbol{\omega}_{r/i} \cdot \boldsymbol{v}_{\texttt{normal}} <= 0$. This test filters most invalid observations away, but in scenarios where self-shadowing may occur, a shadow map calculation is also applied [31]. This, however, requires that the scanned object has been converted into a 3D mesh, which in itself may introduce artifacts if care is not taken.

3.1.3 Data-Driven BRDF Reconstruction

The challenge of fitting a reflectance model to the sparse number of BRDF samples calls for a model with a strong prior. In this study, the data-driven BRDF reconstruction framework of Nielsen et al. [20, 32] is chosen for this purpose, as it is known to work well for problems where only very few BRDF samples are available. The model is based on the MERL database [17] of isotropic BRDFs spanning a wide range of common materials. Using a log-relative mapping of reflectance values, projections in principal component space allows inferring missing observations from existing ones. Effectively the model reconstructs a MERL format BRDF, i.e. a $90 \times 90 \times 180$ bin tabulated isotropic BRDF, from any number of input observations provided. The biggest limitation of this approach is that it requires the measured material to lie within the convex hull spanned by the MERL database. If this is met, under ideal lighting conditions, as little as two images are sufficient to faithfully reproduce a material.

3.2. Simulation of Pipeline

In order to maintain full control of all uncertainties in this fairly complex acquisition pipeline, a simulated pipeline is used to produce realistic HDR images, conforming with a true SL system. We do this by initially picking a ground truth mesh and ground truth measured BRDF from the MERL database. Using these, combined with the true SL system projection matrices, light source positions, and rotation stage positions, an OpenGL renderer is used to produce a series of HDR renderings of the chosen geometry and BRDF as it would have been seen by the SL system. An example of such renderings is shown in figure 3, where 3 different meshes with the "blue-rubber" BRDF applied have been rendered as would be seen by the SL scanning system (although cropped here). With this, the ground truth appearance behind every HDR image is available, allowing for a quantitative evaluation of reconstruction.

3.2.1 Dataset Generation

Four different types of materials and three different types of geometries were chosen to generate the evaluated dataset. Material-wise, four different levels of specularity were chosen, all in different colors, covering the span of material

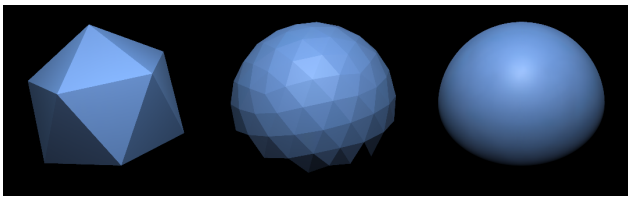

Figure 3: Icospheres with 3 different tessellation levels: 1, 3 and 5. For the highest tesselation level vertex normals have been smoothed.

behavior that would be expected in the real world. The materials are "blue-rubber", "green-metallic-paint", "purple-plastic", and "specular-black-phenolic", with the first having very soft highlights and the last being highly specular (renderings are available in the lower left corner of figures 5–8). As the data-driven BRDF reconstruction model is also based on the MERL database, these four materials were excluded in the model-training. Geometry-wise three different geometries were chosen, spanning the amount of geometric detail that can be expected from real world objects. The geometries are based on an icosphere with increasing tesselation levels and are shown in figure 3. This is motivated by the fact that a sphere naturally covers all possible surface normals, while a plane only covers a single. Thus, the closer the geometry is to a sphere, the more ideal are the BRDF reconstruction conditions from a geometry point of view. Each of the three meshes has been subdivided to consist of roughly 15000 vertices and are scaled to have a diameter of 100 mm in the simulator.

We generate a dataset of HDR images using the materials and geometries described above. Both the scene-light and projector are used as light sources and both cameras are used for observing, see figure 1. In addition, the sample is rotated in 10 steps from $0°$ to $180°$. This gives $n_{\texttt{conf}} = n_{\texttt{rot}} \times n_{\texttt{lights}} \times n_{\texttt{cameras}} = 10 \times 2 \times 2 = 40$ HDR images per material/geometry configuration and $n_{\texttt{total}} = n_{\texttt{conf}} \times n_{\texttt{materials}} \times = n_{\texttt{geometries}} = 40 \times 4 \times 3 = 480$ HDR images in total.

3.2.2 Noise Addition

There are a range of elements in the pipeline depicted in figure 2 that affect the accuracy of the BRDF observations acquired. Any uncertainties in these will obviously cause uncertainties in the BRDF model-fitting. To gain insight into this, four types of uncertainties are investigated:

Vertex position. The precision of the SL system will determine the geometric noise present in a 3D scan. Clearly, as the vertices are projected onto HDR images, any error in position will cause a wrong assignment of radiance value.

Vertex normal. Commonly, surface normals are not a direct product of the 3D acquisition procedure but are estimated afterwards, e.g. based on the spatial distribution of neighboring vertices. This makes the estimation prone to errors, and any wrong orientation of normals will directly influence the reflectance estimate.

Light position. While camera positions are very precisely calibrated, the light position is oftentimes significantly more difficult to determine. The position affects the light direction and thus also the reflectance estimate.

Light intensity. Finally, precise knowledge of the light intensity at any given 3D point in the SL system is not easily obtained. As the light intensity is used to compute the fraction of light reflected off the material surface, it too directly influences the reflectance estimate.

As the evaluated dataset is simulated, the exact system parameters are known. This allows for, prior to processing the data, manually adding a controlled amount of noise to any of the above components. To apply noise in our experiments, we use a normal distribution (Gaussian noise) with the given position or normal as mean and σ is standard deviation. For normals, the noise only applies to the polar angle. To add noise in the case of light intensity, we multiply the intensity by a normal distribution with unit mean and $\sigma/100$ as standard deviation (percentage noise).

3.2.3 Evaluation

Evaluating the quality of an estimated BRDF compared to the ground truth is not trivial and is indeed a research field in itself. In these experiments, both qualitative and quantitative measures are presented:

In-plane reflectance profiles. For qualitative evaluation, $45°$ in-plane reflectance profiles of estimated and ground truth BRDFs are presented. These plots visualize the general shape of the specular highlight as well as parts of the grazing angle behaviour.

Ray-traced sphere renderings. Another qualitative evaluation is using a physically based renderer [21]. Here the BRDFs can be visualized under realistic environment lighting conditions, giving the viewer an impression of how the material would look in the real world. The material examples shown in figures 5–8 are rendered this way.

Tone mapped color difference. Rendered images, using the approach above, of the ground truth and reconstructed BRDFs are compared using the CIEDE2000 color difference perception measure. The HDR images are first scaled to the visible range using Reinhard tonemapping, and gamma correction ($\gamma = 2.2$) at F-stop 0 is applied [1]. The images are then converted to the CIE 1976 L*a*b* color space, and the CIEDE2000 color difference formula [26] (with $[k_L\ k_C\ k_H] = [1\ 1\ 1]$) is used to calculate the color difference ΔE_{00}. The average of all pixel differences is calculated and used as a perceptual similarity measure between

	blue-rubber	green-metallic-paint	purple-paint	specular-black-phenolic
Icosphere 1	0.77 ± 1.02	2.77 ± 2.93	1.56 ± 1.96	1.07 ± 1.13
Icosphere 3	0.37 ± 0.78	2.60 ± 3.11	0.82 ± 1.01	2.50 ± 3.14
Icosphere 5	0.41 ± 0.67	3.00 ± 3.23	0.55 ± 0.75	1.43 ± 1.92
Icosphere 5*	0.52 ± 0.96	5.19 ± 5.20	1.58 ± 1.55	2.29 ± 1.63

Table 1: Errors for increasing geometric detail (icosphere tesselation level). Errors are measured as the average ΔE_{00} color difference between tone mapped renderings of ground truth BRDF and reconstruction. Icosphere 1,3,5 are reconstructions using two light sources, while 5^* are reconstructions using only the projector as light source.

images, and the standard deviation represents the certainty of this number.

4. Results

We report results for BRDF estimation under various noise influences. This includes an evaluation of BRDF estimation performance under three different geometry complexities, followed by an evaluation of performance under influence of uncertainties with respect to vertex position, vertex normal, light source position, and light source intensity. Due to page limitations, some comparisons of in-plane reflectance profiles and renderings have been omitted. A summary of comparisons are reported in tables 1 and 2.

4.1. Geometry Dependency

In order to evaluate how much geometric complexity affects the quality of an estimated BRDF, estimations were carried out on the simulated icospheres with tesselation levels 1, 3 and 5, depicted in figure 3. The estimates were computed under ideal conditions, i.e. no noise added to any of the system components listed in section 3.2.2. In figure 4, quantitative comparisons of the material "purple-paint" are presented in the form of in-plane reflectance profiles and renderings. It may be seen that as geometric detail increases, the quality of reconstruction improves, however the improvement is surprisingly small. In table 1, the results for all four materials are listed, using the ΔE_{00} color-difference measure between ground truth rendering and reconstructed rendering. To the convenience of system designers, errors using icosphere level 5 combined with only the projector as light source is also presented in the bottom row of table 1.

To provide as ideal conditions as possible for the noise simulations, the icosphere level 5 geometry will be used in the following evaluations. For all evaluations, 30 repetitions were carried out to estimate mean and standard deviation of reconstruction. Quantitative comparisons for all materials,

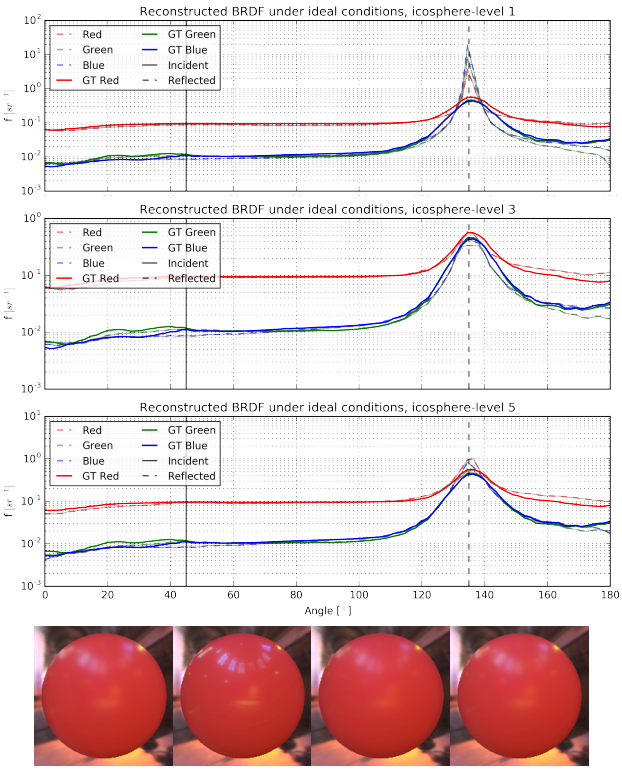

Figure 4: Ideal reconstructions of "purple-paint" material, using icosphere tesselation levels $\{1, 3, 5\}$, shown as $45°$ in-plane profiles. Solid lines indicate ground truth BRDF RGB channels, dashed lines are the reconstructed BRDF RGB channels. Bottom row shows renderings of reference BRDF (left) and reconstructions for the respective icosphere levels.

under various error influences are reported in table 2 using the ΔE_{00} error measure.

4.2. Influence of Vertex Position Noise

Errors in triangulation during the SL scanning procedure directly affect the precision of vertex positions. Commonly, but depending on material, SL scanners have a very high precision in the order of microns [4]. To investigate the sensitivity to vertex positions, all vertices are affected by three relatively large levels of noise prior to projection onto HDR images. The noise is added as a normally distributed noise on the xyz-components of each vertex with standard deviations of $\sigma \in \{1, 3, 5\}$mm. In figure 5, the qualitative evaluations for material "blue-rubber" are presented. As is apparent, grazing angle behavior is greatly affected by vertex uncertainties. This is most likely caused by the fact that even small uncertainties may at grazing angles project a vertex onto the black background, rather than the target sample. Likewise, for very specular materials as "specular-black-phenolic", vertices may miss the very narrow highlight causing errors in estimating the specular reflection.

		blue-rubber	green-metallic-paint	purple-paint	specular-black-phenolic
Ideal		0.41 ± 0.67	3.00 ± 3.23	0.55 ± 0.75	1.43 ± 1.92
Vertex	1mm	0.66 ± 1.15	3.03 ± 3.44	0.91 ± 1.56	2.27 ± 3.37
	3mm	2.50 ± 2.82	3.11 ± 4.17	2.11 ± 3.16	3.41 ± 5.15
	5mm	4.16 ± 4.08	3.24 ± 4.77	3.59 ± 4.32	4.22 ± 5.76
Normal	5°	0.42 ± 0.63	3.00 ± 3.20	0.68 ± 1.03	3.15 ± 5.66
	10°	0.67 ± 0.98	3.08 ± 3.17	0.99 ± 1.70	3.72 ± 6.92
	30°	1.81 ± 2.11	4.70 ± 5.08	2.27 ± 3.27	5.24 ± 8.31
Light Pos.	10mm	0.51 ± 0.72	3.01 ± 3.26	0.62 ± 0.84	2.17 ± 3.32
	25mm	0.73 ± 0.89	2.68 ± 3.03	1.02 ± 1.16	3.05 ± 5.03
	50mm	1.77 ± 1.92	3.14 ± 3.51	1.91 ± 2.27	3.74 ± 6.08
Light Int.	5%	0.64 ± 0.79	3.01 ± 3.29	0.66 ± 0.78	1.90 ± 2.80
	10%	1.00 ± 1.15	3.05 ± 3.38	0.96 ± 0.99	1.98 ± 2.81
	20%	1.75 ± 1.75	3.40 ± 3.74	1.86 ± 2.10	2.27 ± 2.80

Table 2: Errors for different types of noise introduced to the structured light scanner system. Errors are measured as the average ΔE_{00} color difference between tone mapped renderings of ground truth BRDF and reconstruction.

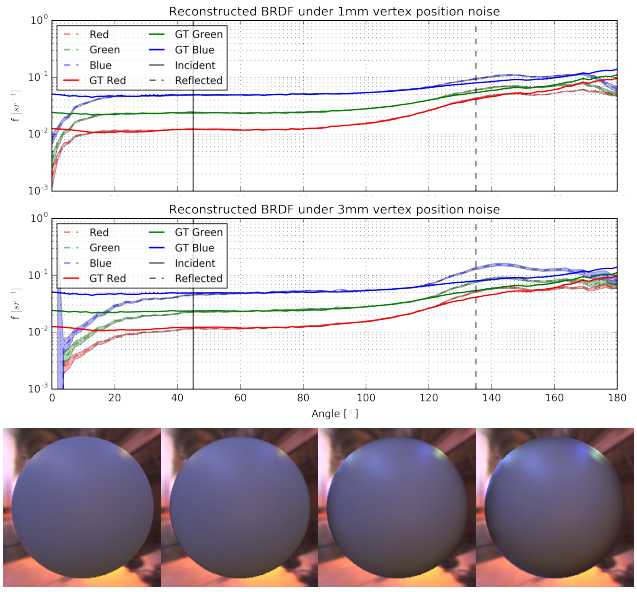

Figure 5: BRDF reconstructions of "blue-rubber" material, for increasing noise added to vertex positions, shown as 45° in-plane profiles. We add Gaussian noise with a standard deviation of $\{1, 3, 5\}$mm. BRDF RGB channels are plotted with solid lines as ground truth and dashed lines as the mean reconstruction. Shaded regions indicate limits for ± 2 standard deviations. Bottom row shows renderings of reference BRDF (left) and mean reconstructions for the respective noise levels. Statistics are based on 30 evaluations.

4.3. Influence of Vertex Normal Noise

As surface normals are often derived from the mesh, they often suffer from large uncertainty. This directly affects the frame of reference in which the BRDF is estimated. To simulate such uncertainties, all normals in the mesh are tilted in a random direction away from the true normal by a normally distributed angle. Three different standard deviations are reported here: $\sigma \in \{5^\circ, 10^\circ, 30^\circ\}$. In figure 6, qualitative evaluations are presented for "purple-paint". Although specular highlights are somewhat affected, it is noteworthy how large an amount of noise we can add to the normals while still obtaining a decent recovery of the material.

4.4. Influence of Light Source Position Noise

As mentioned in section 3.2.2, it may be difficult to determine the precise position of light sources in the SL system. To simulate such uncertainties, normally distributed noise is added to the xyz-components of the light positions (projector and scene-light) with standard deviations of $\sigma \in \{10, 25, 50\}$ mm. In figure 7, the influence of this error is shown for the "green-metallic-paint" material. Surprisingly, even for the relatively large amounts of noise applied here, reconstructions remain very close to the results under ideal conditions as well as the ground truth.

4.5. Influence of Light Source Intensity Noise

Finally, noise applied to the intensity of the light sources (projector and scene light) is applied. Here, the noise is modeled as a normally distributed percentage with a mean of 100%. The standard deviation of the noises applied are $\sigma \in \{5, 10, 20\}\%$. Figure 8 shows the results for the material "specular-black-phenolic". Here, the strong prior of the BRDF reconstruction model almost fully handles the uncertainties in intensity although this property is very tightly coupled to reflectance.

4.6. Summary

Table 2 summarizes the BRDF errors caused by introducing the noise types listed above using the ΔE_{00} error measure. We observe that, not surprisingly, accuracy of vertex positions has a great impact on the quality of the recovered material. Recall that the object size is 100 mm, only a few percent error are enough to throw the BRDF estimate off. On the contrary, variations in surface normals are less influencing than we would have expected, requiring especially for soft materials a lot of noise before throwing the BRDF recovery off. Finally positions and intensities of light sources are seen to have a surprisingly small impact on BRDF reconstructions.

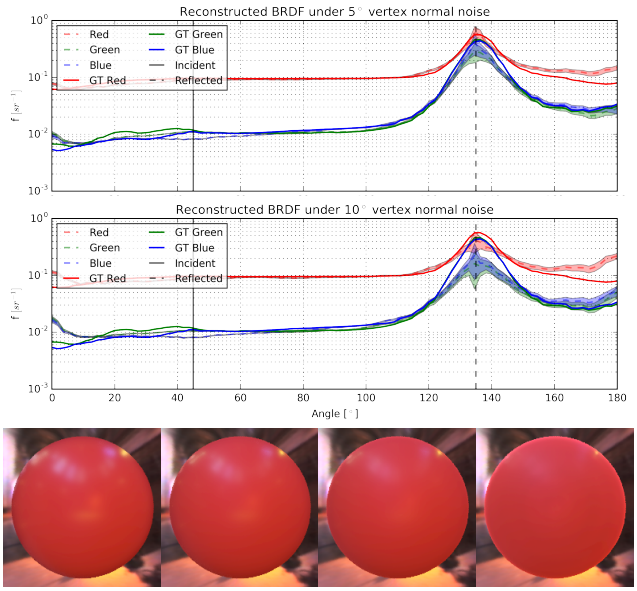

Figure 6: BRDF reconstructions of "purple-paint" material, for increasing noise added to vertex normals, shown as $45°$ in-plane profiles. We add Gaussian noise with a standard deviation of $\{5°, 10°, 30°\}$.

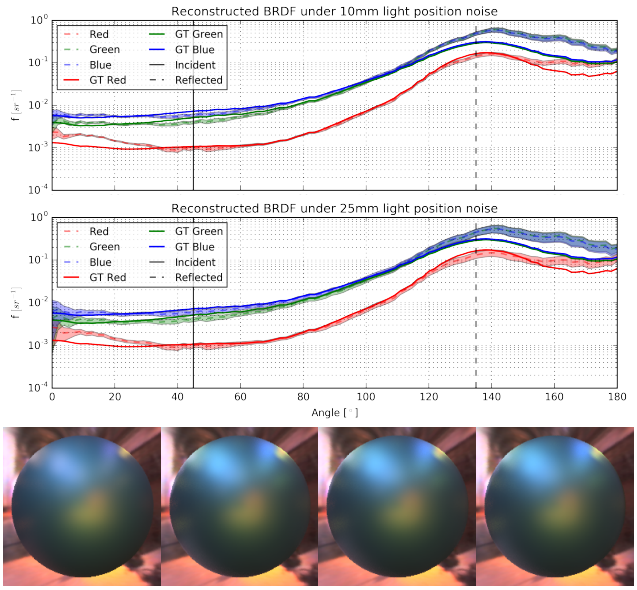

Figure 7: BRDF reconstructions of "green-metallic-paint" material, for increasing noise added to the two light source positions, shown as $45°$ in-plane profiles. We add Gaussian noise with a standard deviation of $\{10, 25, 50\}$mm.

5. Discussion and Conclusion

We investigated how a structured light 3D scanning system can be modified with minimal effort to also estimate

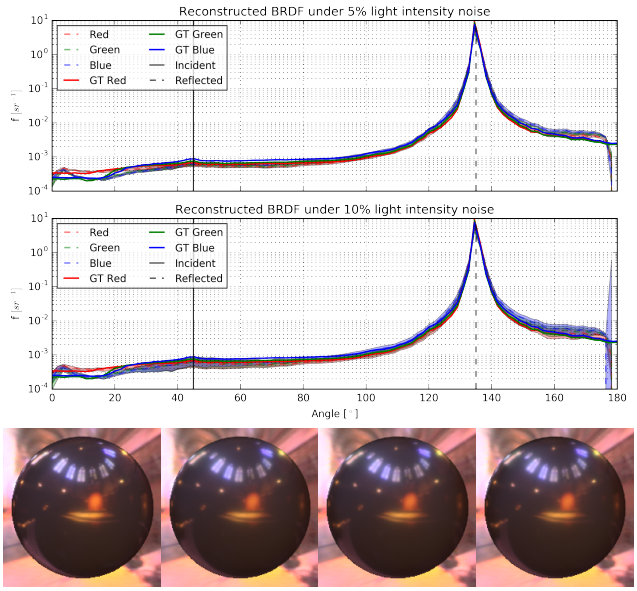

Figure 8: BRDF reconstructions of "specular-black-phenolic" material, for increasing noise added to the two light source intensities, shown as $45°$ in-plane profiles. We add Gaussian noise with a standard deviation of $\{5\%, 10\%, 20\%\}$.

BRDFs. Results indicate that high quality reflectance recovery is in fact possible in such a setup. We carried out a variational study in a simulated environment to investigate how a range of uncertainties in system parameters affect the quality of the estimated reflectance properties. The goal of this study is to provide system designers with a lookup table of system parameter uncertainties required to recover a given material at a given quality-level. This is needed in the design phase of future systems for full appearance acquisition. Tables 1 and 2 provide this information and demonstrate that even under the poor gonioreflectometric conditions provided by a SL system, very high quality reflectance may be recovered. An interesting insight gained here is that uncertainties in surface normals in fact have a smaller impact on the quality of estimated BRDFs than one might have expected. Likewise, uncertainties in illumination properties, including position and intensity, have little influence on the recovered reflectance.

Although the experiments carried out here are only simulated, we believe that they reflect well what can be expected from real world measurements. It has not been the intention with this paper to cover the physical implementation of this pipeline as well as the performance of the approach in real-world scenarios. Nonetheless, the images presented in figure 2 do in fact originate from an actual implementation of the system, demonstrating that it also works in practice. It is our intention to elaborate on these results in the future.

References

[1] F. Banterle, A. Artusi, K. Debattista, and A. Chalmers. *Advanced High Dynamic Range Imaging: Theory and Practice*. AK Peters (CRC Press), Natick, MA, USA, 2011.

[2] J. F. Blinn. Models of light reflections for computer synthesized pictures. *Proceedings of ACM SIGGRAPH 77*, 11(2):192–198, July 1977.

[3] P. E. Debevec and J. Malik. Recovering high dynamic range radiance maps from photographs. In *Proceedings of SIGGRAPH 97*, pages 369–378. ACM/Addison-Wesley, 1997.

[4] E. R. Eiríksson, J. Wilm, D. B. Pedersen, and H. Aanæs. Precision and accuracy parameters in structured light 3-D scanning. *International Archives of the Photogrammetry, Remote Sensing and Spatial Information Sciences*, XL-5/W8:7–15, 2016.

[5] J. Geng. Structured-light 3d surface imaging: a tutorial. *Advances in Optics and Photonics*, 3(2):128–160, 2011.

[6] L. Gomes, O. R. P. Bellon, and L. Silva. 3D reconstruction methods for digital preservation of cultural heritage: A survey. *Pattern Recognition Letters*, 50:3–14, December 2014.

[7] M. Halioua and H.-C. Liu. Optical three-dimensional sensing by phase measuring profilometry. *Optics and Lasers in Engineering*, 11(3):185–215, 1989.

[8] R. I. Hartley and A. Zisserman. *Multiple View Geometry in Computer Vision*. Cambridge University Press, second edition, 2004.

[9] S. Hill, S. McAuley, A. Conty, M. Drobot, E. Heitz, C. Hery, C. Kulla, J. Lanz, J. Ling, N. Walster, F. Xie, A. Micciulla, and R. Villemin. Physically based shading in theory and practice. In *ACM SIGGRAPH 2017 Courses*, July 2017.

[10] M. Holroyd, J. Lawrence, and T. Zickler. A coaxial optical scanner for synchronous acquisition of 3d geometry and surface reflectance. *ACM Transactions on Graphics (Proceedings of SIGGRAPH 2010)*, 29(4):99:1–99:12, July 2010.

[11] K. Ikeuchi and K. Sato. Determining reflectance properties of an object using range and brightness images. *IEEE Transactions on Pattern Analysis and Machine Intelligence*, 13(11):1139–1153, November 1991.

[12] J. Krzesłowski, R. Sitnik, and G. Mączkowski. Integrated three-dimensional shape and reflection properties measurement system. *Applied optics*, 50(4):532–541, February 2011.

[13] E. P. Lafortune, S.-C. Foo, K. E. Torrance, and D. P. Greenberg. Non-linear approximation of reflectance functions. In *Proceedings of SIGGRAPH 1997*, pages 117–126. ACM/Addison-Wesley, 1997.

[14] H. Lensch, J. Kautz, M. Goesele, W. Heidrich, and H.-P. Seidel. Image-based reconstruction of spatial appearance and geometric detail. *ACM Transactions on Graphics*, 22(2):234–257, April 2003.

[15] J. Lu and J. Little. Reflectance function estimation and shape recovery from image sequence of a rotating object. In *Proceedings of International Conference on Computer Vision (ICCV 1995)*, pages 80–86. IEEE, 1995.

[16] S. R. Marschner, S. H. Westin, E. P. Lafortune, K. E. Torrance, and D. P. Greenberg. Image-based BRDF measurement including human skin. In *Rendering Techniques 1999*, pages 131–144. Springer, 1999.

[17] W. Matusik, H. Pfister, M. Brand, and L. McMillan. A data-driven reflectance model. *ACM Transactions on Graphics (Proceedings of SIGGRAPH 2003)*, 22(3):759–769, 2003.

[18] J. B. Nielsen, E. R. Eiríksson, R. L. Kristensen, J. Wilm, J. R. Frisvad, K. Conradsen, and H. Aanæs. Quality assurance based on descriptive and parsimonious appearance models. In *Workshop on Material Appearance Modeling (MAM 2015)*, pages 21–24. The Eurographics Association, June 2015.

[19] J. B. Nielsen, J. R. Frisvad, K. Conradsen, and H. Aanæs. Addressing grazing angle reflections in Phong models. In *SIGGRAPH Asia 2014 Posters*, page 43. ACM, 2014.

[20] J. B. Nielsen, H. W. Jensen, and R. Ramamoorthi. On optimal, minimal BRDF sampling for reflectance acquisition. *ACM Transactions on Graphics (Proceedings of SIGGRAPH Asia 2015)*, 34(6):186:1–186:11, November 2015.

[21] M. Pharr, W. Jakob, and G. Humphreys. *Physically Based Rendering: From Theory to Implementation*. Morgan Kaufmann, third edition, 2016.

[22] B. T. Phong. Illumination for computer generated pictures. *Communications of the ACM*, 18(6):311–317, June 1975.

[23] S. Rusinkiewicz. A new change of variables for efficient BRDF representation. In *Rendering Techniques '98 (Proceedings of EGWR 1998)*, pages 11–22, 1998.

[24] Y. Sato, M. D. Wheeler, and K. Ikeuchi. Object shape and reflectance modeling from observation. In *Proceedings of SIGGRAPH 1997*, pages 379–387. ACM/Addison-Wesley, 1997.

[25] C. Schwartz, R. Sarlette, M. Weinmann, and R. Klein. DOME II: A parallelized BTF acquisition system. In *Workshop on Material Appearance Modeling (MAM 2013)*, pages 25–31. The Eurographics Association, June 2013.

[26] G. Sharma, W. Wu, and E. N. Dalal. The CIEDE2000 color-difference formula: Implementation notes, supplementary test data, and mathematical observations. *Color Research & Application*, 30(1):21–30, 2005.

[27] R. Sitnik, J. KrzesŁ, M. Grzegorz, et al. Archiving shape and appearance of cultural heritage objects using structured light projection and multispectral imaging. *Optical Engineering*, 51(2):021115–1, 2012.

[28] K. E. Torrance and E. M. Sparrow. Theory for off-specular reflection from roughened surfaces. *Journal of the Optical Society of America*, 57(9):1105–1114, September 1967.

[29] B. Tunwattanapong, G. Fyffe, P. Graham, J. Busch, X. Yu, A. Ghosh, and P. Debevec. Acquiring reflectance and shape from continuous spherical harmonic illumination. *ACM Transactions on graphics (Proceedings of SIGGRAPH 2013)*, 32(4):109, 2013.

[30] M. Weinmann and R. Klein. Advances in geometry and reflectance acquisition (course notes). In *Proceedings of SIGGRAPH Asia 2015 Courses*. ACM, November 2015.

[31] L. Williams. Casting curved shadows on curved surfaces. *Computer Graphics (Proceedings of SIGGRAPH 78)*, 12(3):270–274, August 1978.

[32] Z. Xu, J. B. Nielsen, J. Yu, H. W. Jensen, and R. Ramamoorthi. Minimal BRDF sampling for two-shot near-field reflectance acquisition. *ACM Transactions on Graphics (Proceedings of SIGGRAPH Asia 2016)*, 35(6):188:1–188:12, November 2016.

[33] S. Zhang and P. S. Huang. Novel method for structured light system calibration. *Optical Engineering*, 45(8):083601–083601, 2006.

[34] Z. Zhang. A flexible new technique for camera calibration. *IEEE Transactions on Pattern Analysis and Machine Intelligence*, 22(11):1330–1334, 2000.